International Journal of Fatigue 101 (2017) 36–44

Contents lists available at ScienceDirect

International Journal of Fatigue

journal homepage: www.elsevier.com/locate/ijfatigue

Characterization of bending vibration fatigue of WBD fabricated Ti-6Al-4V

Benjamin Ellyson [a,*], Nejib Chekir [b], Mathieu Brochu [b], Myriam Brochu [a]

[a] École Polytechnique de Montréal, Montréal, Québec, Canada
[b] McGill University, Montréal, Québec, Canada

ARTICLE INFO

Article history:
Received 11 October 2016
Received in revised form 4 March 2017
Accepted 22 March 2017
Available online 4 April 2017

Keywords:
Titanium
Wire beam deposition
Additive manufacturing
Vibration fatigue
Fractography

ABSTRACT

Wire Beam Deposition (WBD) is an Additive Manufacturing (AM) technique used in creating thick or thin geometries from wire stock. This technique has recently generated interest in the aerospace field for its potential to fabricate high performance, defect-free materials while minimizing post-processing and achieving high buy-to-fly ratios. Also, vibration fatigue is a technique used to generate fatigue data representative of turbine blade and vane High Cycle Fatigue (HCF) failure conditions. In this work, cantilever vibration bending fatigue of Ti-6Al-4V produced by WBD is studied. Tensile strength results are also briefly presented. Specifically, the Failure Probability Distribution (FPD) for 10^7 cycles is quantified using the Dixon-Mood staircase method. Additionally, fractography and microstructure data are used to supplement fatigue results and understand the failure mechanisms of the studied material states. Lastly, SLM fatigue and 3D vibrometry data are used to perform a comparative analysis of vibration fatigue performance of these two AM processes. The study finds that high deposition speeds lead to high fatigue performance. The material deposited at 454.66 mm/min had a performance nearly isotropic in nature and surpassing that of the reference material (AMS 4911). It was also found that WBD produced Ti-6Al-4V has a slightly lower crack nucleation resistance than the best-case SLM material, while showing a narrower spread for failure probability.

1. Introduction

AM technologies have been gaining attention over the past years for their promise of heightened material and time efficiency. These technologies also unlock advanced topological design methods and permit the generation of complex geometries unattainable with previous fabrication paradigms. As a novel process, AM still lacks the required data and model-based understanding needed to maintain a high level of confidence necessary for aerospace applications. In fact, it has been stated [1] that high inter- and intra-process variability has been the main factor holding back the industrial implementation of AM. Also, Frazier [1] adds that the development of in-process control systems and batch-based certification processes are key in the future of AM and that these must rely on extensive material properties databases and model-based understanding of mechanical behaviour.

WBD is a direct energy deposition process wherein material (in wire form) is directly added to a melt pool maintained by a laser (or an e-beam). Through this method, thin or thick geometries can be build up continuously or in a layer-by-layer method [2] to generate shell sections with minimal material waste. WBD is a promising candidate for industrial application for the capacities mentioned above, allowing for lower buy-to-fly ratios in fabricating complex thin-sectioned parts. It has also been shown to be able to produce material states that either equal or surpass the performance of conventional counterparts with little to no post-processing, as demonstrated for Ti-6Al-4V [2,3]. Kelly and Kampe [4] showed how heat extraction through previously deposited layers allows for cyclic heat treatment causing *in situ* martensitic decomposition and microstructural evolution. This intrinsic heat-treatment combined with mainly defect-free solidification means that minimal post-deposition heat treatment is necessary [2–5], contrarily to Selective Laser Melting (SLM). On the other hand, WBD is known to have a lower resolution than other AM techniques, so that as-deposited features cannot be as small. Also, the absence of a powder bed does not permit the addition of sacrificial support structures, which further limits the geometric freedom for as-deposited features. Lastly, in terms of microstructure, the lower cooling rates typically associated with WBD leads to coarser grain structures.

* Corresponding author.
E-mail address: benjamin.ellyson@gmail.com (B. Ellyson).

http://dx.doi.org/10.1016/j.ijfatigue.2017.03.045
0142-1123/

The minimal post-processing required for above standard performance can also be extended to conventional fatigue performance [6]. Although little work has been published on the subject, WBD fatigue characterization is crucial if it is to be used to generate fatigue critical aerospace parts. Brandl et al. and Baufeld et al. [2,3] investigated HCF smooth surface fatigue strength of WBD samples and found that different orientations of the Build Direction (BD) relative to solicitation had different fatigue strengths. It was reported that crack nucleation resistance perpendicular to the BD was the greatest. However, since only a single material state was investigated, it is still unknown how other deposition parameters affect HCF performance and if any interaction effect is present between anisotropy of fatigue strength and deposition states. Also, failure analysis was only briefly addressed and failure mechanisms were only partially identified. Furthermore, vibration fatigue performance of these materials has not been reported to the best knowledge of the author.

To address the use of this AM technology for the fabrication of fatigue critical cold-section components in gas turbine applications, a vibration-based fatigue method is used to characterize the HCF behaviour of thin-section samples. As mentioned by Scott-Emuakpor et al. [7], conventional fatigue data is misrepresentative of actual HCF solicitation conditions of turbine blades, where high rotational speeds generate high frequency and generally mixed-mode resonant stress states. Thus, by means of the vibration-based fatigue technique, it is possible to generate steady state resonant solicitation close to actual HCF failure conditions for these types of applications. In addition, other advantages of this fatigue testing technique are shorter testing times due to the high frequency of resonant loading and the flexibility of stress distribution due to the multiplicity of mode shapes for any given geometry.

This publication is a continuation of a previous study [8] that is based on the same test methodology and analysis. First, the fabrication of the samples and the microstructural characterization is presented. Afterwards, the vibration-based fatigue test method is quickly summarized, having already been presented in the previous publication. The ensuing results are analyzed using the Dixon-Mood staircase method and show that a higher deposition speed leads to near isotropic performance exceeding wrought material counterparts. Additionally, the results of the fractography study supplement the discussion, enabling an understanding of the link between microstructure, fatigue performance and failure mechanisms.

2. Fabrication

The samples were deposited using a LAWS 1000 automated welding system equipped with a 1 kW YAG solid fiber laser. The deposition uses Ti-6Al-4V ELI wire and was completed in an open argon-flooded box. Further details on the deposition parameters are subject to limited disclosure. However, any further information can be found in the manuscript pertaining to the process/microstructure optimization study performed on this process [9].

Some microstructural parameters play an important role in determining fatigue performance of Ti-6Al-4V, namely the α plate width in lamellar structures [10]. Samples having differing microstructures were fabricated using separate sets of deposition parameters. To synthesize the two different sets of deposition parameters, the deposition speed was used as a calculated quantity. For clarity purposes, the two speeds are referred to as high and low henceforth, and they are equal to 454 mm/min and 83 mm/min, respectively.

WBD materials are known to have directional macrostructures and anisotropic mechanical properties, including fatigue performance [6]. The effect of BD relative to the 1st principal stress is studied here. The BD is varied according to the orientation in which the samples are extracted from the plates. The two orientations studied are shown in Fig. 1.

Before sample extraction, all plates were stress relieved as per AMS 2801. This heat treatment was chosen so as to conserve the effect of deposition parameters on the microstructure, in other words to minimize microstructural evolution while still alleviating residual stress [9].

A total of 5 plates per deposition speed were used to obtain the samples necessary for both build orientations: 3 plates for the Z direction samples, for a total of 12 samples; 2 plates for the X direction, for a total of 10 samples. This lead to 10 plates being used to generate 44 samples in total. The different sample sets are presented in Table 1.

The samples were ground flat to a final thickness of 1.59 mm and cut to specification (see Fig. 2) using Electrical Discharge Machining (EDM). Following this, the samples were polished using the following steps:

1. Vibratory tumbling in ceramic media for a preliminary sanding and to round corners;
2. Sanding down using progressively finer SiC papers to 1200 grit;
3. Polishing using alumina suspension down to 5 μm.

3. Material characterization

The tested materials' microstructures were characterized by observing polished sections. Sections were cut from plates for both speeds and in turn mounted and polished using colloidal silica for microstructural observation. Both optical and Scanning Electron Microscopes (SEM) were used on etched (Kroll's etchant) and unetched samples respectively. Only SEM images are presented herein. Also, optical imaging techniques were used to observe the macrostructural features of the unaltered plates. Fig. 4 was produced using a blind reader in a typical document scanner and Fig. 7 was taken with a digital camera.

3.1. Reference material

The WBD vibration fatigue data is compared to the same reference data as the one used in Ellyson et al. [8]. The reference series is produced from a cold-rolled annealed plate of Ti-6Al-4V as specified in AMS 4911. The AMS 4911 minimum tensile properties can be found in Table 2. Also, the nominal composition range of the reference material is presented in Table 3 as specified by AMS 4911.

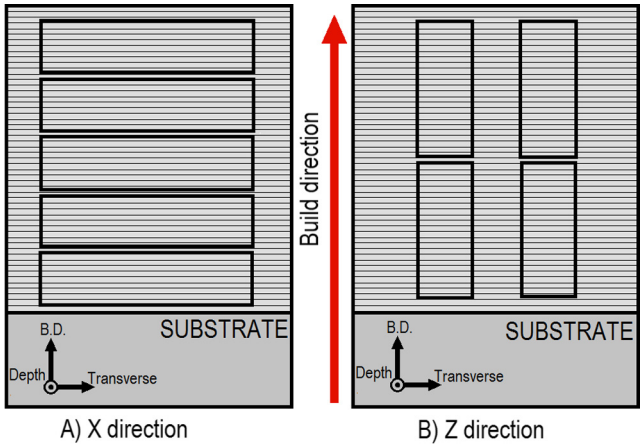

Fig. 1. Schematic representation of the extraction strategy used to obtain samples along two different BDs (not to scale).

Table 1
Table showing the states of samples tested. The number of samples tested in each series is presented in parenthesis.

Direction of σ_{11}	∥ to Z	∥ to X
Deposition speed	83 mm/min (12) 454 mm/min (12)	83 mm/min (10) 454 mm/min (10)

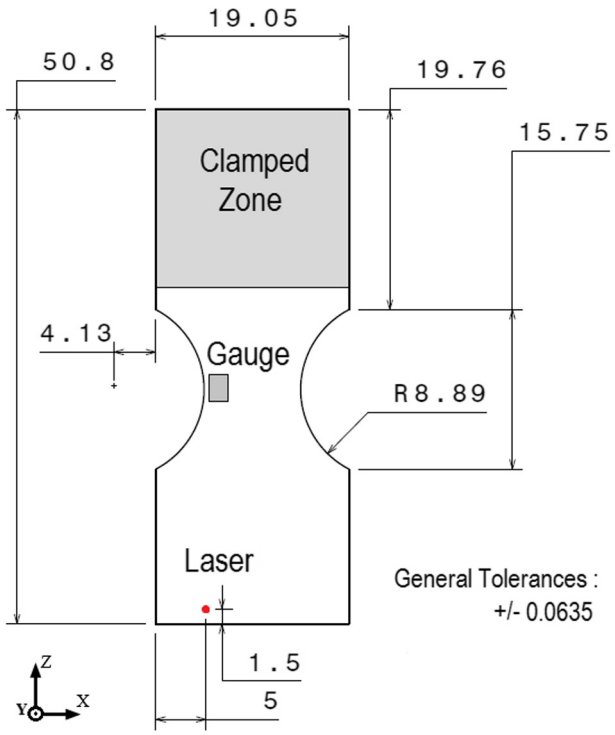

Fig. 2. Technical drawing of sample geometry showing position of instrumentation and clamped zone (measurements are in mm).

Table 2
Table presenting the minimum tensile properties (yield strength (S_y), ultimate tensile strength (S_u) and elongation (EL)) of the reference series as specified in AMS 4911.

Material specification	S_y (MPa)	S_u (MPa)	EL (%)
AMS 4911	869	920	10

In all cases, the reference material respects these specifications as verified by the mill certificate and third-party testing. Lastly, published data is widely available for AMS 4911 annealed sheet so that a reference point for the fatigue resistance at 10^7 cycles can be easily obtained. The raw reference material data are subject to limited disclosure.

This plate presents a typical microstructure of nearly equiaxed primary α grains of 15 μm in diameter evenly distributed in a retained β matrix, as can be seen in Fig. 3. The α grains are slightly elongated in the rolling direction.

3.2. WBD material

Microstructural investigation revealed, for all WBD sample states, that the samples exhibit a columnar macrostructure

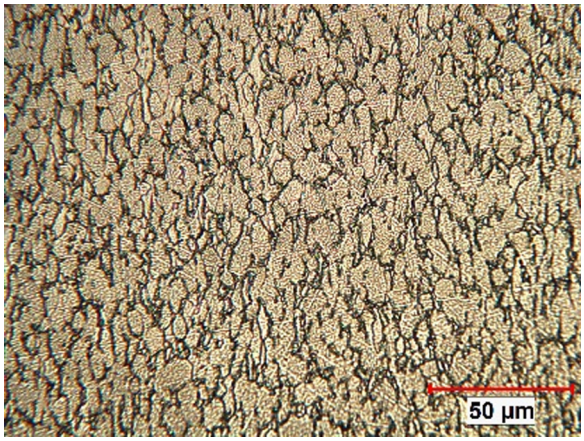

Fig. 3. Typical microstructure of AMS 4911 plate used for reference samples. Rolling direction is aligned with the top-bottom direction of the image.

typically found in AM of Ti-6Al-4V due to rapid solidification and epitaxial growth from previous layers [4,3,11,12]. Fig. 4 shows an optical image highlighting the columnar microstructure of a high deposition speed plate, clearly showing the grains aligned with the BD. The grains are prior-β grains formed in the temperature interval between solidification and the β transus during cooling. The inside of these grains is then transformed into a fully $\alpha - \beta$ structure through the subsequent thermal cycling caused by the following layers being deposited [4]. A typical $\alpha - \beta$ basketweave microstructure was found, as shown in Figs. 5 and 6 for the low and high speed microstructures, respectively. The α plate average width in the steady-state region varies slightly from 0.5 μm to 0.8 μm [9] for the high to low speed, respectively.

Also, it is interesting to note that, for the low deposition speed, the residence time in the β temperature domain was long enough to cause recrystallization of the columnar grains partway through the build, leading to a change in prior-β columnar grain orientation from parallel to the BD to perpendicular to the BD, as presented by Chekir et al. [9]. As it can be seen in Fig. 7, the columnar grains are vertically oriented at the beginning of the deposition but change orientation abruptly partway through the deposition due to the heat input of the following deposition layers [9]. It can also be seen that the vertical columnar grains tend to slant in the direction of deposition slightly before the transition, as highlighted by the green circles in Fig. 7.

4. Fatigue testing method

The method uses an electromagnetic shaker to maintain a steady state resonant vibration in order to fatigue a cantilever sample. A closed-loop control system was used where the displacement was measured by a 1D laser vibrometer in order to control the magnitude and frequency of the force generated by the shaker. The feedback loop also allowed resonant frequency tracking providing a means to automatically detect the formation of a crack and stop the testing. A crack that initiates and propagates in a sample lowers the natural resonant frequency and increases dissipation in the system [13,14]. In this study, the stopping criterion was chosen to be 5% of the original resonant frequency, which represents a crack of roughly 5 mm. In all cases, sample failure

Table 3
Table presenting the composition for a Ti-6Al-4V plate as per AMS 4911 specifications.

Element	Al (wt%)	V (wt%)	Fe (wt%)	O (wt%)	C (wt%)	N (wt%)	Ti (wt%)
AMS 4911	5.5–6.75	3.5–4.5	0.3 min	0.2 min	0.08 min	0.05 min	Balance

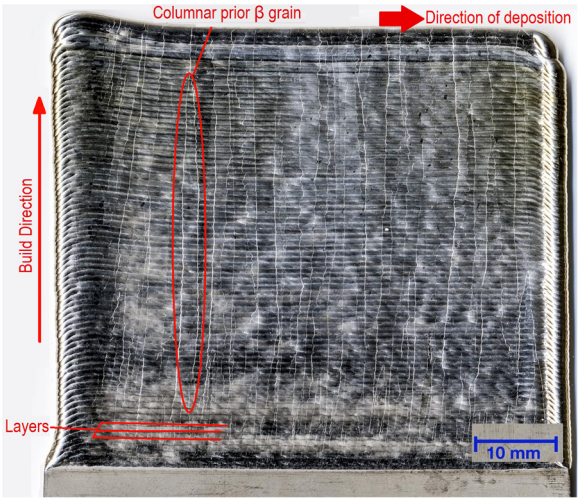

Fig. 4. Optical image showing the columnar prior-β grains of a high deposition speed plate.

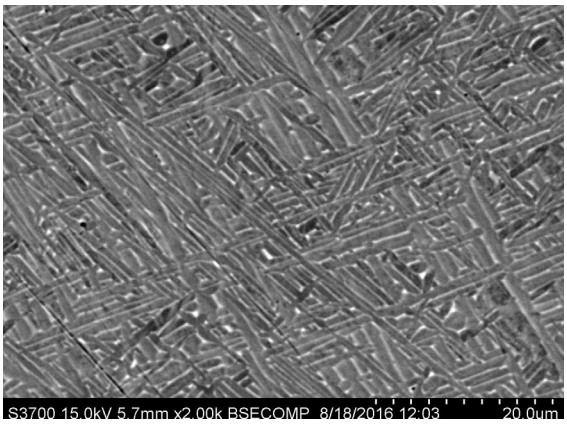

Fig. 5. Microstructure of the WBD low (83 mm/min) speed material.

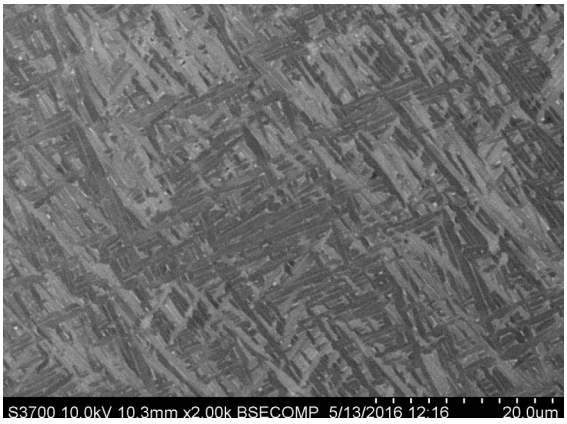

Fig. 6. Microstructure of the WBD high (454 mm/min) speed material.

was visually confirmed once the test automatically stopped. All things being equal, this stopping criterion was used for all samples and allows for an equivalent fatigue life in all samples to be considered for fatigue resistance analysis.

Moreover, being a displacement controlled technique, it was necessary to use a calibration factor to calculate the strain amplitude in the location of crack nucleation [13]. This was accomplished through the use of strain gauges positioned as shown in Fig. 2. The calibration is averaged over short cycle counts (typically 2000) at low displacement and different amplitudes.

This testing technique was used in concordance with the staircase method of Dixon and Mood [15] to determine the controlling parameters (mean and standard deviation) of the FPD for 10^7 cycles.

A more detailed explanation of the methodology as well as validation of different experimental aspects are presented in the previous manuscript of this study [8]. For additional information on the technique and underlying theory, please refer to the works of Seidt, George et al., Wang et al., Yun et al., and Scott-Emuakpor et al. [16,13,17,14,18,7].

5. Results and discussion

5.1. Tensile properties

The relative tensile properties shown in Table 4 are taken from Chekir et al.'s work [9]. The data from each column were divided by the value of the reference series to obtain relative property values and thus are referred to as "normalized". An aspect of note is the nearly isotropic mechanical strengths demonstrated by these materials. In contrast, the elongation shows pronounced anisotropy at low speeds. The reason behind this difference in elongation is likely due to the anisotropic macrostructure, i.e. the columnar prior-β grains, as low elongation is usually a sign of microstructural heterogeneities. This aspect is discussed in Section 5.2 and in Chekir et al.'s work [9]. It seems that columnar grains that are aligned with the deposition layers lead to premature rupture and low elongation, pointing to the controlling aspect of these microstructural heterogeneities. For both high speed directions and the low speed in the X direction, this aspect is present when compared to the reference materials, which is known to be highly homogeneous and isotropic, but almost absent when compared amongst themselves. However, the most pronounced difference in elongation is seen for the low speed in the Z direction. Logically, this behaviour points to microstructural heterogeneities oriented along the fracture plane (XY plane in Fig. 2 or transverse-depth plane in Fig. 1). This conclusion is reinforced by the fatigue results as shall be shown in Section 5.2. Lastly, it must be mentioned that the reference material's tensile properties meet or exceed the AMS 4911 minimum specifications.

5.2. Fatigue results and statistical analysis

Table 5 shows the parameters characterizing the FPD for 10^7 cycles, in other words the mean and standard deviation. The performance of each series is assumed to follow a normal distribution [15].

The results show that the low speed exhibits a lower performance in the X direction when compared to the reference series and an equal performance in the Z direction. The X direction's mean stress amplitude is only 64% of that in the Z direction. This is the largest difference in performance among all tested series. Three aspects are thought to contribute to the lower performance of the low speed compared to the reference and high speed, and the lower overall performance in the X direction:

1. The change of columnar grain orientation from parallel to the BD to perpendicular to the BD;
2. The presence of long α grains at columnar prior-β grain boundaries;
3. The coarsening of the microstructure by longer high-temperature residence times.

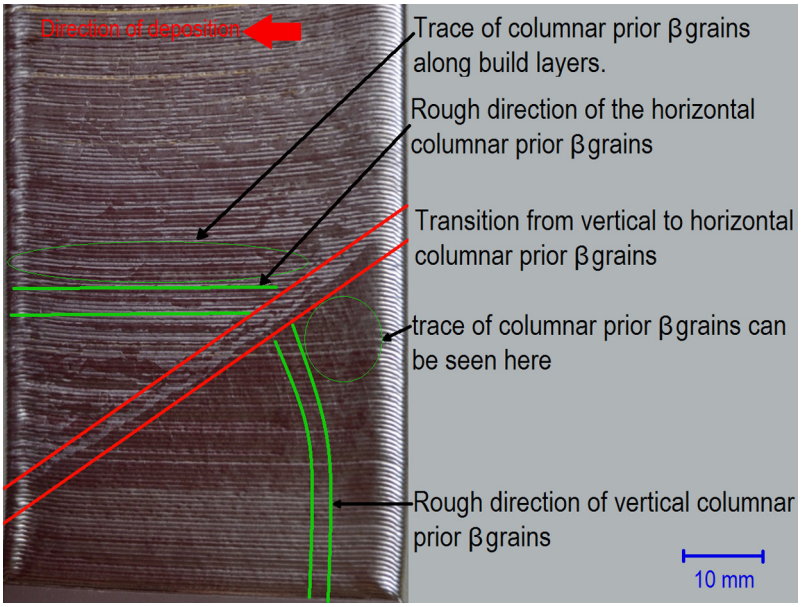

Fig. 7. Optical image showing the columnar prior β grains and the transition of direction of a low deposition speed plate. This image was taken by Nejib Chekir.

Table 4
Table presenting the normalized tensile properties (yield strength (S_y), ultimate tensile strength (S_u) and elongation (EL)) of investigated materials normalized against the reference series (AMS 4911). Each of the values of S_y and S_u are divided by the absolute value of the reference series' S_y, so that the ratio of S_y to S_u can be compared. The EL values are all divided by the absolute values of the references series elongation. This data was generated by Nejib Chekir.

Speed	BD	Normalized S_y (%)	Normalized S_u (%)	Normalized EL (%)
Reference		100	105	100
Low	Z	88	94	23
	X	90	95	50
High	Z	98	107	66
	X	103	109	51

Table 5
Table presenting the mean and standard deviation of the FPD at 10^7 cycles normalized against the performance of the reference series, i.e. all values are divided by the mean stress amplitude of the reference series (AMS 4911). The mean represents the stress amplitude at which 50% of the population will survive 10^7 cycles.

Speed	BD	Normalized mean (%)	Normalized standard deviation (%)	Sample size
Reference		100	4.9	14
Low	Z	100	4.0	11
	X	64	7.0	10
High	Z	111	2.9	9
	X	109	3.0	9

First off, the fact that the low speed plates contain a mix of columnar grains both parallel and perpendicular to the BD (Fig. 7) leads to a higher chance of obtaining a weakened orientation from a single plate, depending on the zone in which the sample is extracted, as illustrated in Fig. 8. This is due to the recrystallization behaviour outlined by Chekir et al. [9]. The low deposition speed leads to enough excess heat to allow for a recrystallization of the layers. This effect is especially present in the X direction for the low speed since the reoriented columnar grains are intersected by the notch and tangent to the notch root. Logically, this also contributes to increase the spread of results for this direction. Secondly, the long α grains at columnar prior-β grain boundaries should logically play a role in the nucleation of a crack. It can be seen as a preferential site for nucleation since the crystallographic orientation is conserved along its length. It would stand to logic that one of these long grains favourably orientated at the surface leads to premature crack nucleation within the context of a "weakest link" behaviour. These elongated phases are known to follow the prior-β grain boundaries [3,12]. As shown in Figs. 7 and 8, the low speed X direction samples contain a mix of these columnar prior-β grains both perpendicular and parallel to the BD. The reoriented columnar grains generate an altogether higher statistical chance of long α grains traversing high stress zone at the root of the notch. Thirdly, it is quite obvious that the excess heat leads to the presence of coarsened α plates, as stated in Section 3.2, and this in turns produces a weaker crack nucleation resistance as the α plate width is known to be a controlling factor in Ti-6Al-4V fatigue behaviour [19,10]. In summary, it can be said that for the low speed samples, the recrystallization behaviour produces a material where macro and microstructural heterogeneities (i.e. layer bands and columnar interface α) are all aligned, wherein all contribute to weaker crack nucleation resistance.

When the high speed alone is considered, the BD does not significantly contribute to fatigue performance. As such, this material state can be considered isotropic for HCF performance. Also, the results show that this material state exceeds the performance of

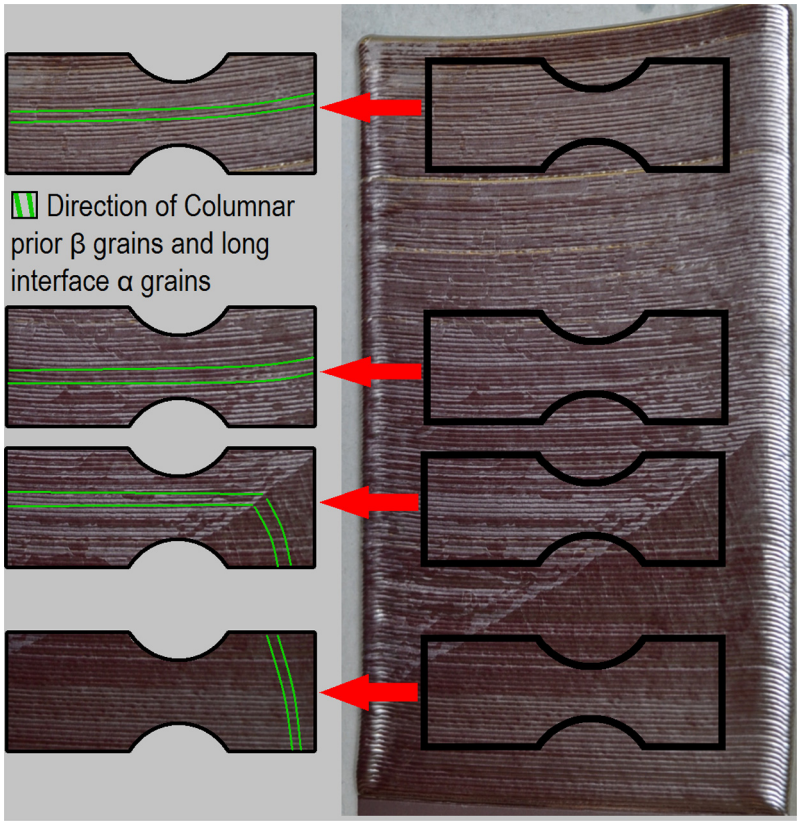

Fig. 8. Illustration of the effect of mixed columnar prior-β grain orientations and sample extraction from plates on the resulting macrostructure of the samples tested. Note how the bottom samples contain a mix of columnar orientations and the top samples contain only columnar grains aligned with the layers.

conventional cold-rolled counterparts by 10% when both directions are averaged.

Considering the effect of both parameters, it must be noted that a strong interaction is present between both the BD and speed. Clearly, the influence of the BD disappears at a higher speed, leading to the conclusion that deposition speed affects the amount of anisotropy demonstrated. The relationship between the two parameters is inverse, where higher speeds leads to lessened anisotropy. In this study, the high speed is fast enough that complete isotropy is obtained.

Also, even though the Dixon-Mood method is known to grossly over-estimate the standard deviation of the FPD for small samples [20], the results in Table 5 allow to conclude relative differences at least. In this sense, the high speed can also be said to lower the spread of the FPD relative to the low speed. This is to be expected in light of the more consistent macrostructure and finer microstructure found in the high speed samples.

Moreover, Fig. 9 shows the mean stress amplitude at 10^7 cycles normalized against their yield and ultimate strengths for all tested series. It is interesting to note that the trends emerging in this graph echo the relative performance seen in Table 5. In other words, the strongest performing series also have the highest fatigue performance relative to their respective yield strengths. Also of note, the Z low speed series has a fatigue to yield strength ratio higher than the reference series even though they performed equally in fatigue trials (Table 5). This indicates that the yield and ultimate strength of this series is lower than that of the reference series.

Interestingly, Fig. 9 highlights the effect of the experimental setup used in this study on the fatigue crack nucleation resistance found during this investigation. The black line in the graph indicates typical conventional axial fatigue performance at 20 Hz for

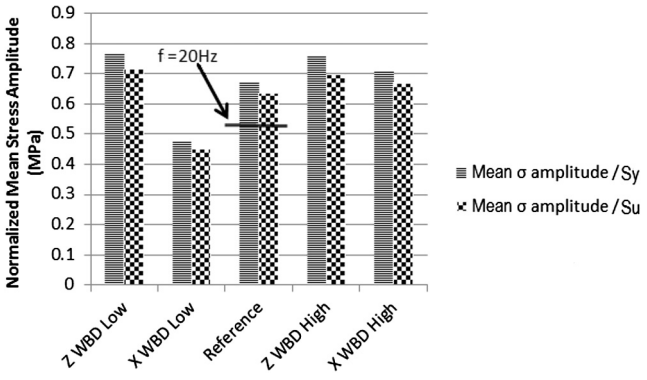

Fig. 9. Graph of the mean failure stress amplitude at 10^7 cycles normalized to the yield strength (S_y) and ultimate tensile strength (S_u) of each material state. For each series, the horizontally striped and checkered bars represent the mean stress amplitude for 10^7 cycles divided by each series' yield strength and ultimate tensile strength, respectively.

AMS 4911. The difference between this line and the value of the reference series presented in Fig. 9 is mainly due to an increase in the fatigue crack nucleation resistance for the samples tested in this study. Among other things, Ti-6Al-4V is known to demonstrate a sensitivity to loading frequency under certain conditions for tensile [21] and fatigue behaviour [22,23]. There are also other phenomena strongly affecting the fatigue results presented herein such as the bending stress gradient through the thickness of the samples, the stress concentration gradient from the shallow notch and the surface stress state of the thin samples, to name only the most prevalent. All of these effects combine to provide a roughly 20% increase in fatigue resistance for the reference material

(AMS 4911) when compared to literature data. These data points are found to be roughly 500 MPa for fatigue crack nucleation resistance of AMS 4911 under conventional fully reversed ($R = -1$) axial loading at 10^7 [24] and roughly 510 MPa for vibration bending fatigue crack nucleation resistance at 10^7 cycles. The last value of 510 MPa was extrapolated from the closest known experimental results in literature, which are Scott et al.'s reference values obtained at 1800 Hz [7].

5.3. Fractography

First off, crack initiation, when identifiable, was always attributed to microstructural features at the surface while defect-based crack initiation was absent. This agrees with the microstructural investigation presented in Section 3, since no process-induced defects were found in the material, e.g. porosity, inclusions, oxides, etc. These results also corroborate findings by Baufeld et al. [3], who reported microstructural nucleation sites at the surface.

Figs. 10a and 11a present a general view of two selected fracture surfaces from the high and low speeds respectively. In both figures, propagation lines visibly converge to the crack nucleation sites, which are presented at higher magnification in Figs. 10b and 11b. Both figures show crack nucleation at what is believed to be an α colony intersected by the surface. These results were inferred from the fractography results published by Sterling et al. [25] for Laser Engineered Net Shape (LENS) heat-treated specimens, wherein they demonstrate crack nucleation at an α colony cut by a surface. In fact, Chekir et al. [9] characterized the steady-state microstructure and layer bands, where the latter were shown to be populated mainly by α colonies, while the former contained only a small proportion of colonies. These microstructural results are shared in most WBD research work [4,2,3]. Also, it can be seen from Fig. 12 that the colony size is consistent with the size of nucleation sites found on fracture surfaces. In light of these results, the only logical candidate for such a microstructural feature acting as crack nucleation site is an α colony.

As per Hall's analysis of titanium alloys' crack initiation behaviour [19], a weakest link philosophy holds true for titanium alloys, where the size of the largest similarly oriented crystallographic domain determines crack nucleation resistance. In his publication, Hall highlights colonies, large texture domains or prior-β grain size for β-processed alloys as potential weakest links. Prior-β grain width can be excluded already since fatigue performance corresponding to this particular domain size (above $1mm$) does not agree with presented results. Furthermore, β-processed alloys typically present prior-β grains which are entirely populated by aligned α platelets, which is not the case for the WBD materials in this study. In fact, the most likely candidate is colony size. Since colonies present a larger domain where platelets are similarly aligned, they are considered to be the microstructural features presenting the longest slip length [10] in the material, thus leading to the shortest crack nucleation time. It can be summarized that a favourably aligned colony intersected by a surface presents a preferential crack nucleation site when compared to a zone of randomly oriented platelets (as in the case of a basketweave structure).

Lastly, an important result of the study pertains to the failure mechanisms with respect to each variable investigated. In all failed samples, failure mechanisms appear constant across both directions and both speeds. It was impossible to correlate a change of failure mechanisms to a variation of deposition speed or BD, since most sample showed similar crack nucleation behaviour. As such, it is hypothesized that the differences in fatigue behaviour presented herein are due to statistical differences in colony population, size and orientation with respect to the surface and fatigue solicitation. As mentioned in Section 5.2, the X direction low speed altogether poor fatigue performance is most likely due to the recrystallization behaviour leading to a higher colony population and thus a higher statistical chance of having a favourably oriented colony be intersected by a sample surface.

6. Comparative study of vibration fatigue behaviour of SLM and WBD Ti-6Al-4V

In Ellyson et al.'s publication [8], SLM vibration fatigue behaviour was characterized and analyzed, allowing a comparative analysis to be made between the two AM techniques. Since this paper is a continuation of the project presented in Ellyson et al.'s previous work, equivalent data and analysis are produced for both AM processes.

Firstly, in order to validate a comparative analysis of fatigue performance from a purely material perspective, tensile and fatigue behaviours must be compared. A 3D Scanning Laser Doppler Vibrometer (3D-SLDV) is used to obtain dynamic strain distribution of the WBD samples in the first bending mode. This data is compared to numerical simulations and to 3D-SLDV reference and SLM data generated in Ellyson et al. [8].

When comparing simulation results and reference material data to WBD sample scans, similar conclusions to those presented in Ellyson et al. [8] are found. In summary, differences in dynamic strain behaviour were identified as a slight level of asymmetry and are thought to be due to material dissimilarities, although the scale of these differences are found to be small enough (i.e. within error margins) not to influence predicted dynamic and fatigue behaviour, especially due to the shallow notch.

In light of these conclusions, differences in fatigue behaviour can be rationalized from a material's point of view. The fatigue results for the FPD at 10^7 cycles for the SLM samples in both BDs and having undergone a Stress Relief (SR) or a Hot Isostatic Pressing (HIP) are presented in Table 6 for reference purposes.

When SLM fatigue performance (Table 6) is compared to WBD sample performance (Table 5), it can be seen that the SR series exhibits premature crack nucleation, even relative to the worst performing WBD series. Microstructural characterization and fractography reveal that the martensitic and porous microstructure of the SLM SR samples is responsible for this low performance. In Ti-6Al-4V, martensite is known to exhibit low ductility and high strength when compared to $\alpha - \beta$ basketweave structures [10,26,6]. This characteristic combined with the stress concentration effect of porosity at the surface leads to a worst-case scenario and low crack nucleation resistance. The essentially defect-free material of the WBD samples allows microstructure to dictate crack nucleation leading to a fatigue behaviour comparable to wrought material counterparts and far surpassing SLM SR performance.

Alternatively, the SLM HIP samples show a fatigue performance surpassing even the best case of the WBD samples. Interestingly, microstructural characterization shows that the SLM HIP samples exhibit a microstructure that is on average much coarser than both WBD deposition speeds considered, so that this difference cannot be explained purely in terms of α plate width. When the results of the fracture analysis are considered, the SLM HIP samples show that crack nucleation is mainly dominated by residual pores left unclosed from the HIP cycle, while WBD failure is dictated by colonies intersected by a machined surface. The pores responsible for crack nucleation in the SLM HIP samples were on average never larger than 5 μm, which is a length scale comparable to the dominant microstructural phase, while for the WBD samples, colony size is on average 10 μm and varies quite widely from this measure. The relative size difference in these microstructural features

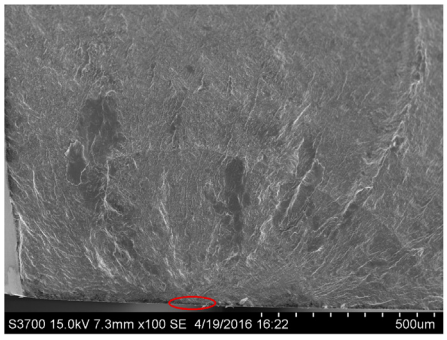

(a) General view of fracture surface of a high speed series sample, showing the crack initiation site circled in red.

(b) Magnification of the red circled area in Figure 10a showing the α colony where the crack nucleated. Note that the initiation site is circled for clarity.

Fig. 10. Fracture surface of a high speed series sample investigated in this study.

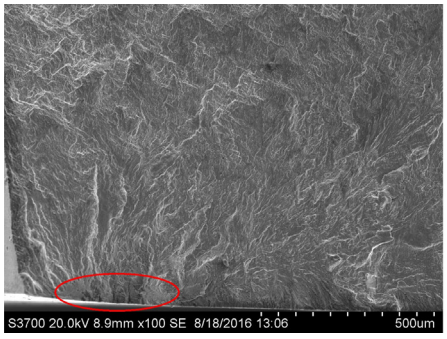

(a) General view of fracture surface of a low speed sample, showing the crack initiation site circled in red.

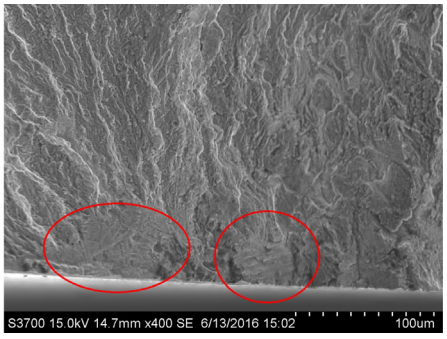

(b) Magnification of the red circled area in Figure 11a showing the α colony where the crack nucleated. Note that the initiation site is circled for clarity.

Fig. 11. Fracture surface of a low speed series sample investigated in this study. Magnifications differing from Fig. 10 are presented for purpose of clarity and due to the difference scales of presented features.

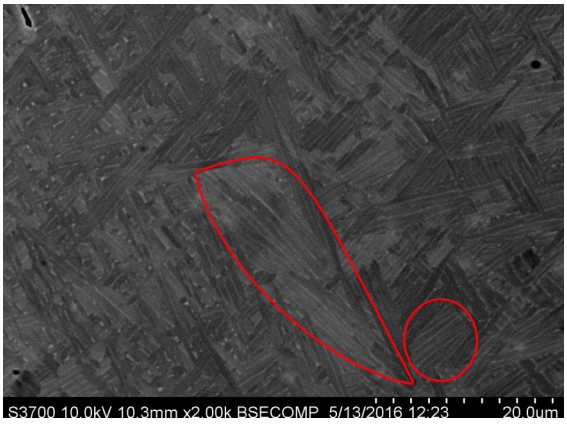

Fig. 12. SEM image showing α platelet colonies of a high deposition speed plate. The red perimeters delineate separate examples of colonies of different size. (For interpretation of the references to colour in this figure legend, the reader is referred to the web version of this article.)

identified in the fractographic study as main culprits for crack nucleation seems to explain the difference in relative fatigue performance.

From a processing point of view, SLM leads to a highly homogeneous martensitic microstructures due to typically high cooling rates. Additionally, the subsequent HIP cycle temperature is maintained under the β transus. This effectively limits the thermal activation of diffusional mechanisms in the microstructure, thus hindering the growth of deleterious features such as colonies and elongated inter-β α grains that are found in WBD samples. This process-specific difference in thermal cycling highlights the trade-off between SLM and WBD with respect to microstructural homogeneity and resulting fatigue crack initiation behaviour.

Table 6
FPD parameters (mean and standard deviation) for SLM samples divided by the mean of the reference series FPD. These results are presented as a reminder for the comparative analysis and are taken from Ellyson et al. [8].

Series	Normalized mean (%)	Normalized standard deviation (%)
Z SLM SR	47	6.4
X SLM SR	57	6.4
Z SLM HIP	118	4.8
X SLM HIP	136	4.8

7. Conclusion

It has been shown in this article that WBD is a viable AM process for generating HCF critical aerospace hardware since the high deposition speed demonstrated a crack nucleation resistance that exceeds conventional cold-rolled counterparts (AMS 4911). Additionally, it has been shown that this deposition state shows an isotropic behaviour. These results add to the case supporting WBD use in aerospace industrial applications since high deposition speeds lead to shorter building times and a microstructure that maximizes tensile properties and HCF performance.

Moreover, investigation of the effect of low deposition speeds leads to a higher scatter and lowered mean stress amplitude, mainly due to longer residence time in the β domain and slower heat extraction. As stated in Chekir et al. [9], deleterious macro and microstructural evolution ensues.

Fractographic data supports the fatigue data in the conclusions on parameter effects and shows that WBD is mainly guided by defect-free crack nucleation. For all identifiable initiation sites, the crack nucleated at microstructural sites or surface irregularities. In essence, WBD shows no extraordinary crack nucleation mechanisms in comparison to conventional lamellar Ti-6Al-4V and these findings corroborate those presented in other publications [2,3,6].

Additionally, in Section 6, the difference in fatigue performance between WBD and SLM materials is rationalized by microstructural characterization and fractography data. This section concludes that the difference in fatigue performance can be totally accounted for by the different failure mechanisms shown to be present in each material state, i.e. porosity for SLM and α colonies for WBD.

Future work on this process should strive to quantify the effect of the location of sample extraction on a plate. It is well known that WBD builds show transient microstructures near boundaries. It is not well understood how these microstructure gradients affect fatigue performance in general. These effects are not studied in this project. A study utilizing an analysis of covariance between HCF behaviour and position in the build is key to a complete understanding of the effects of transient deposition such as the first or last layer or near the edges in non-continuous depositions.

Acknowledgments

The author would like to acknowledge the "Consortium de recherche et innovation en aéronautique du Québec" (CRIAQ), the École Polytechnique de Montréal and McGill University, as well as Bell Helicopter Textron Canada, Bombardier, Edmit, GE, Héroux-Devtek, Liburdi, MDA and Pratt Whitney Canada for their project contribution under the CRIAQ MANU-601/NSERC CRD grant. Also, the author would like to thank GE Aviation for the use of their testing equipment, Liburdi for the production of the samples and Héroux-Devtek for the use of their SEM.

References

[1] Frazier WE. Metal additive manufacturing: a review. J Mater Eng Perform 2014;23(6):1917–28. http://dx.doi.org/10.1007/s11665-014-0958-z. URL <http://link.springer.com/10.1007/s11665-014-0958-z>.
[2] Brandl E, Baufeld B, Leyens C, Gault R. Additive manufactured Ti-6Al-4V using welding wire: comparison of laser and arc beam deposition and evaluation with respect to aerospace material specifications. Phys Proc 2010;5:595–606.
[3] Baufeld B, Brandl E, Van der Biest O. Wire based additive layer manufacturing: comparison of microstructure and mechanical properties of Ti–6Al–4V components fabricated by laser-beam deposition and shaped metal deposition. J Mater Process Technol 2011;211(6):1146–58.
[4] Kelly S, Kampe S. Microstructural evolution in laser-deposited multilayer Ti-6Al-4V builds: Part I. Microstructural characterization. Metall Mater Trans A 2004;35(6):1861–7.
[5] Wang F, Mei J, Wu X. Microstructure study of direct laser fabricated Ti alloys using powder and wire. Appl Surf Sci 2006;253(3):1424–30.
[6] Li P, Warner D, Fatemi A, Phan N. Critical assessment of the fatigue performance of additively manufactured Ti–6Al–4V and perspective for future research. Int J Fatigue 2016;85:130–43.
[7] Scott-Emuakpor O, Holycross C, George T, Knapp K, Beck J. Fatigue and strength studies of titanium 6Al–4V fabricated by direct metal laser sintering. J Eng Gas Turbines Power 2016;138(2):022101.
[8] Ellyson B, Brochu M, Brochu M. Characterization of bending vibration fatigue of slm fabricated Ti-6Al-4V. Int J Fatigue 2017;99:25–34.
[9] Chekir N, Gauvin R, Brodusch N, Sixsmith JJ, Brochu M. Effect of travel speed and post deposition heat treatments in laser wire deposition of thin Ti-6Al-4V buildups, Part I: microstructure characterization. Chekir N, Tian Y, Sixsmith JJ, Brochu M. Effect of travel speed and post deposition heat treatments in laser wire deposition of thin Ti-6Al-4V buildups, Part II: mechanical properties.
[10] Lütjering G. Influence of processing on microstructure and mechanical properties of (α+β) titanium alloys. Mater Sci Eng: A 1998;243(1–2):32–45. http://dx.doi.org/10.1016/S0921-5093(97)00778-8.
[11] Brandl E, Michailov V, Viehweger B, Leyens C. Deposition of Ti–6Al–4V using laser and wire, Part I: microstructural properties of single beads. Surf Coat Technol 2011;206(6):1120–9.
[12] Brandl E, Schoberth A, Leyens C. Morphology, microstructure, and hardness of titanium (Ti-6Al-4V) blocks deposited by wire-feed additive layer manufacturing (ALM). Mater Sci Eng: A 2012;532:295–307.
[13] George TJ, Seidt J, Shen M-HH, Nicholas T, Cross CJ. Development of a novel vibration-based fatigue testing methodology. Int J Fatigue 2004;26(5):477–86.
[14] Yun G, Abdullah A, Binienda W. Development of a closed-loop high-cycle resonant fatigue testing system. Exp Mech 2012;52(3):275–88.
[15] Dixon WJ, Mood AM. A method for obtaining and analyzing sensitivity data. J Am Stat Assoc 1948;43(241):109–26.
[16] Seidt JD. Development of a novel vibration based high cycle fatigue test method Ph.D. thesis. The Ohio State University; 2001.
[17] Wang Y-C, Hoechbauer T, Swadener J, Misra A, Hoagland R, Nastasi M. Mechanical fatigue measurement via a vibrating cantilever beam for self-supported thin solid films. Exp Mech 2006;46(4):503–17.
[18] Scott-Emuakpor O, George T, Beck J, Schwartz J, Holycross C, Shen MH, et al. Material property determination of vibration fatigued DMLS and cold-rolled nickel alloys. In: ASME Turbo Expo 2014: turbine technical conference and exposition. American Society of Mechanical Engineers; 2014. p. V07AT28A008–V07AT28A008.
[19] Hall J. Fatigue crack initiation in alpha-beta titanium alloys. Int J Fatigue 1997;19(93):23–37.
[20] Pollak RD. Analysis of methods for determining high cycle fatigue strength of a material with investigation of Ti-6Al-4V gigacycle fatigue behavior. Tech. rep., DTIC Document; 2005.
[21] Nicholas T. Tensile testing of materials at high rates of strain. Exp Mech 1981;21(5):177–85.
[22] Morrissey R, McDowell D, Nicholas T. Frequency and stress ratio effects in high cycle fatigue of Ti-6Al-4V. Int J Fatigue 1999;21(7):679–85.
[23] Takeuchi E, Furuya Y, Nagashima N, Matsuoka S. The effect of frequency on the giga-cycle fatigue properties of a Ti–6Al–4V alloy. Fatigue Fract Eng Mater Struct 2008;31(7):599–605.
[24] ASM, Fatigue and fracture; 1996.
[25] Sterling AJ, Torries B, Shamsaei N, Thompson SM, Seely DW. Fatigue behavior and failure mechanisms of direct laser deposited Ti–6Al–4V. Mater Sci Eng: A 2016;655:100–12.
[26] Leuders S, Thöne M, Riemer A, Niendorf T, Tröster T, Richard H, et al. On the mechanical behaviour of titanium alloy TiAl6V4 manufactured by selective laser melting: Fatigue resistance and crack growth performance. Int J Fatigue 2013;48:300–7.